Edge Effect on the Photodetection Ability of the Graphene Nanocrystallites Embedded Carbon Film Coated on p-Silicon

*Xi Zhang, Da Peng, Zezhou Lin, Wencong Chen, and Dongfeng Diao**

A sensitive photodetector of graphene nanocrystallites embedded carbon (GNEC) film coated on p-silicon has been proposed. Different from the conventional growth mode of graphene, GNEC film contains a large amount of vertically grown graphene nanocrystallites (GNs). Edges of GNs act as electron trapping centers, increasing the ability to capture electrons. Different types of films are prepared under various deposition biases (20, 40, 60, and 80 V), which have different density of edges (N_{edge}). Edge entrapment improves the photocurrent responsivity of 40 V film (high N_{edge}) to 0.401 A W^{-1}, compared with 0.126 A W^{-1} of 20 V film (amorphous, no N_{edge}) and 0.194 A W^{-1} of 80 V film (low N_{edge}). A high specific detectivity of 1.34×10^{12} cm $Hz^{1/2}$ W^{-1} is exhibited at zero bias. GNs maintain a charge transport channel, which makes it have a fast response time $\tau_{rise} = 260$ ns.

Photodetectors are an indispensable core component in many modern precision analytical, measurement and diagnostic instruments.[1] Photodetectors fabricated using heterojunctions are superior to those fabricated with homojunctions in the aspect of low dark noise, etc.[2] Graphene is a hexagonal 2D film composed of a single layer of sp^2 hybrid carbon atoms,[3] which has the potential ability of fast photoresponse.[4] The preparation methods of graphene mainly include mechanical peeling method, SiC epitaxial growth method, redox method, and chemical vapor deposition method (CVD). However, these methods require strict conditions and hardly produce large area samples. In comparison, carbon films are relatively easy to prepare in large areas and low-cost, and have the potential to become a new type of optoelectronic device for industrial production.

In the past, the research on amorphous carbon film mainly focused on its microstructure, electronic structure, and preparation method. For example, thin tetrahedrally coordinated amorphous carbon (ta-C) films have been grown using a filtered vacuum arc.[5] H. A. Yu, prepares an amorphous carbonaceous film at a low temperature by a chemical vapor deposition (CVD) method.[6] It exhibits a degree of transparency and good electrical conductivity, indicating that carbon materials can be used as materials for microelectronic devices.[7] There are several studies on photoelectric response characteristics of carbon films.[8,9] For example, V. S. Veerasamy reported the photovoltaic behavior and spectral response of n-type (nitrogen-doped) tetrahedral amorphous carbon (ta-C)/p-type crystalline silicon heterojunction photodiodes.[10] In 2012, Xue et al.[11] prepared Pd-doped amorphous carbon (a-C) film/SiO_2/Si heterojunction by sputtering system and tested its substrate resistivity, light-induced resistance effect[12] and photoconductivity.[13] However, the a-C film/Si photodetector shows a low responsivity below 0.18 A W^{-1}.

Recently, a graphene nanocrystallites embedded carbon film (GNEC) was obtained by using electron cyclotron resonance (ECR) plasma sputtering technique. The nanostructure of the carbon film can be modulated by adjusting the low energy electron irradiation energy (V_{dep}) during deposition. The embedded graphene nanocrystallites contribute a high density of edges to the film. Edges and defects were considered to generate extra energy states near Fermi-level[14,15] and show different behaviors from bulk materials, such as serving as trapping centers in photovaltic processes.[15,16] The GN edges significantly improves the performance of the GNEC film in terms of electromagnetics,[17–19] surface friction,[20] and photoelectricity.[14,21]

In this paper, we fabricated GNEC film/p-Si heterojunction photodiode by growing carbon films on p-silicon with low energy electron irradiation, and tested its photoelectric properties. Different types of films were prepared under various deposition biases (20, 40, 60, and 80 V), which have different density of edges (N_{edge}). We investigate the relation between the N_{edge} and the photo-response performances.

Experimental Details: The GNEC film was deposited on 4-inch p-Si wafer (0.5 mm thickness) using ECR sputtering techniques. We have detailed description of the sputtering system in our previous research work.[22] The chamber was pumped to 4.10×10^{-4} Pa. A microwave of 500 W power is delivered to the chamber to generate a plasma, and the mirror confinement magnetic field was applied to enhance the plasma density. During the deposition, high-purity argon gas is introduced. Ar^+ ions sputter the carbon material to the substrate. A positive deposition bias (V_{dep}) is applied to the substrate to attract

Dr. X. Zhang, D. Peng, Z. Lin, Dr. W. Chen, Prof. D. Diao
Guangdong Provincial Key Laboratory of Micro/Nano Opto-Mechatronics Engineering
Institute of Nanosurface Science and Engineering
Shenzhen University
Shenzhen 518060, China
E-mail: dfdiao@szu.edu.cn

The ORCID identification number(s) for the author(s) of this article can be found under https://doi.org/10.1002/pssr.201800511.

DOI: 10.1002/pssr.201800511

electrons. Adjusting V_{dep} can control the nanostructures of graphene nanocrystals (GNs) on the carbon film. The thicknesses of the GENC films are about 70 nm. In this work, we prepared GNEC films at V_{dep} of 20, 40, 60, and 80 V. The nanostructures of the carbon films were transmission electron microscopy (TEM, JEOL, JEM-3200FS) and analyzed with Raman spectroscopy (HORIBA, HR-Resolution; wavelength of 532 nm).[23]

GNEC film coated on p-Si forms a heterojunction, as shown in **Figure 1**a. UV-lithography was used to deposit a finger-type 50 nm-thick gold electrode on the surface of the GNEC film. A 50 nm-thick flat gold electrode was deposited on the back of the p-Si substrate. *I–V* curves were measured using a Keithley 4200-scs semiconductor characterization analyzer. The Lakeshore TTPX cryogenic probe station covered by the integrated darkroom is used as an electrode contact. Spectral response was measured by a set-up of white light source, monochromator, chopper, and lock-in amplifier. A xenon light in the visible to near-infrared (300–1100 nm) range was used as white light source. The xenon lamp light was dispersed by a monochromator (precision of 0.5 nm) and the average power is at the order of 10 $\mu W\,nm^{-1}$. To measure the response time, the open circuit voltage signal picked up by the probe tip was recorded by a wideband oscilloscope (Keysight DSOX3104T).

Results and Discussion: Figure 1 shows the diagram of the GNEC film/p-Si heterojunction and the characterization of the GNEC films. The structure diagram of the GNEC film/p-Si heterojunction is shown in Figure 1a. The effective area of the device is $5 \times 5\,mm^2$. In the top finger-type electrode, the spine (≈300 μm) and branch (≈150 μm) shapes of the electrode are designed to be wedge shaped with a distance of about 500 μm between the branches. A 50 nm-thick flat gold electrode was deposited on the back of the p-Si substrate. A diode bias (V_{diode}) is applied on the p-Si substrate against the GNEC film. Figure 1b shows high resolution transmission electron microscopy (TEM) image of the cross-section sample of 40 V film. The vertical thickness of the GNEC film on Si can be measured as ≈72 nm. The lateral thickness of the cross-section sample is about 100 nm fabricated by focused ion beam (FIB) and a protection layer was deposited on top. The protective layer is a layer of platinum material having a thickness of 2 μm deposited on the surface of the sample by an auxiliary gas injection system associated with a FIB-SEM analysis system prior to focused ion beam etching process. The role of the

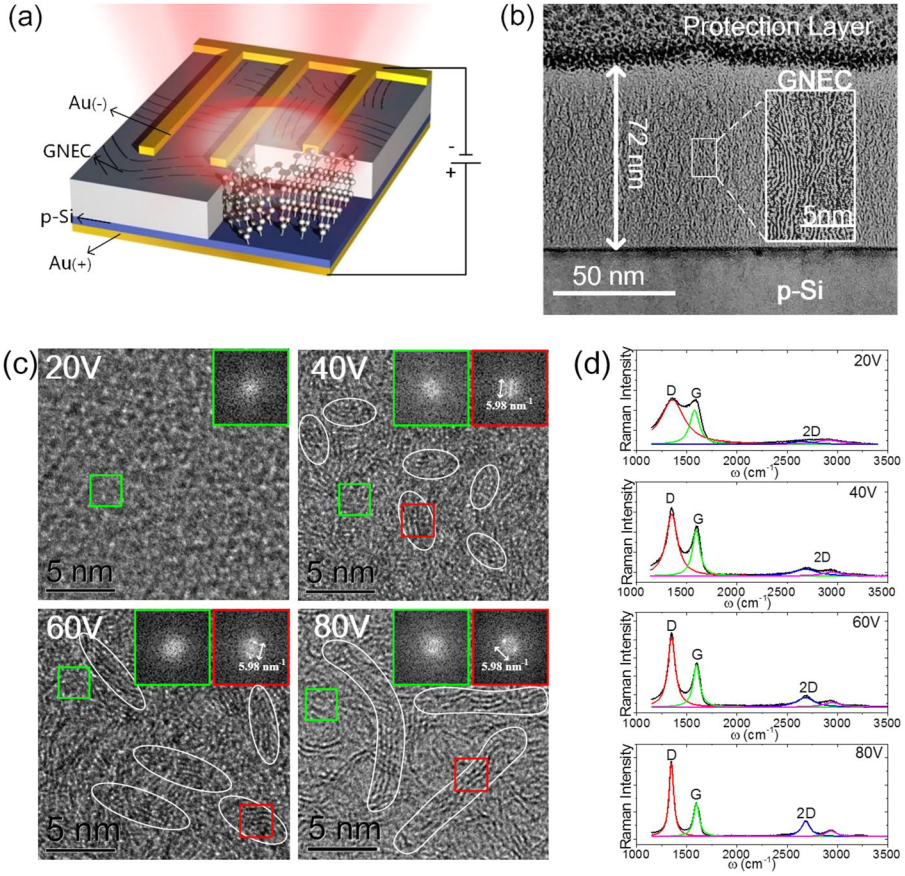

Figure 1. a) Schematic diagram of a GNEC film/p-Si heterojunction device. The effective area of the device is $5 \times 5\,mm^2$. Diode bias (V_{diode}) is applied on the p-Si substrate against the GNEC film. b) High-resolution TEM image of the cross-section sample of 40 V film prepared by focused ion beam. c) Top-view TEM images of carbon films deposited at a V_{dep} of 20, 40, 60, and 80 V. As the V_{dep} energy increases, the GN boundary width increases. d) Raman spectra of GNEC films with V_{dep} at 20, 40, 60, and 80 V.

protective layer is to prevent the surface of the sample from being etched during the FIB etching process and from being damaged during TEM test. Vertical alignment of GNs distributed among amorphous carbon film was obtained despite of small angle deviations and the fact that TEM image is the superposition of 100 nm-thick cross-section film.

Figure 1c shows top-view TEM images of GNEC films deposited at $V_{dep} = 20$, 40, 60, and 80 V. The red and green boxes in the figure mark the areas with or without GN, and their Fast Fourier Transform (FFT) pictures. The white circle is used to indicate the boundary of the GN on the GNEC film, and the average size of the white circle indicates the width of the GN boundary. No obvious in-layer structure was observed at $V_{dep} = 20$ V. The GNEC film prepared by $V_{dep} = 40$ V was observed to start to appear with a small width of GN (≈3 nm), which was densely distributed over the GNEC film. At $V_{dep} = 60$ V, the GN on the GNEC film began to be crisscrossed, and the GN width was increased to an average of 7 nm. At $V_{dep} = 80$ V, it can be clearly observed that a large width of GN (≈12 nm) is distributed on the GNEC film.

As shown in Figure 1d, Raman spectroscopy was performed on GNEC films deposited at $V_{dep} = 20$, 40, 60, and 80 V. By measuring the Raman spectrum of the GNEC film, it is possible to judge the number of layers of graphene,[24] the stacking method, the number of defects and the structure and properties of the edge structure. In the Raman spectrum of the GNEC film, the D peak, the G peak and the 2D peak were used to characterize the structural defects and edges, the number of layers of the GN, and the stacking pattern of the graphene layer. The ratio of the D peak/G peak I_D/I_G is used to reflect the edge structure of the GNEC film, and the 2D peak is used to reflect the crystallinity of the GNEC film.[25] The 2D band becomes sharper with the increase of the V_{dep} in these spectra, suggesting the existence of graphene layers since it arises from the two-phonon involved double resonance Raman process[26] of graphene layer. At $V_{dep} = 20$ V, after peak separation, the G peak is weak relative to the D peak and the 2D peak is not obvious, indicating that the GNEC film has an amorphous structure and a low crystallinity. At $V_{dep} = 40$ V, the D peak G peak is distinct and the 2D peak has small undulations, indicating that a small width GN and a high density edge structure begin to appear. At $V_{dep} = 60$ V, the increase in the crystallinity of the graphene interlayer leads to a further increase in the width of the GN, and the increase in the width of the GN causes the G peak to decrease. At $V_{dep} = 80$ V, the film forms a more ordered layered structure with an average GN width of 12 nm.

As shown in **Figure 2**a, the photogenerated current of the GNEC film/p-Si was tested by laser incident power (from 10 to 100 mW) under a laser of 785 nm wavelength. When the incident power is 10 mW, the photogenerated current of the GNEC film/p-Si is 3.9 mA at zero bias, and the GNEC film/P-Si generates a photocurrent of 4 mA at a bias of −2 V. The smaller the incident power laser irradiation is, the easier the photocurrent reaches to saturation under reverse bias. Unlike Graphene/n-Si[24] exhibiting a drastically photocurrent depression at $V_{diode} = 0$ V due to the Dirac cone of grapehne, the GNEC film/p-Si show a good photocurrent at $V_{diode} = 0$ V due to the natural pn junction formation between electron-trapped GN and p-Si. The reverse bias can raise GN's Fermi level to open up available energy

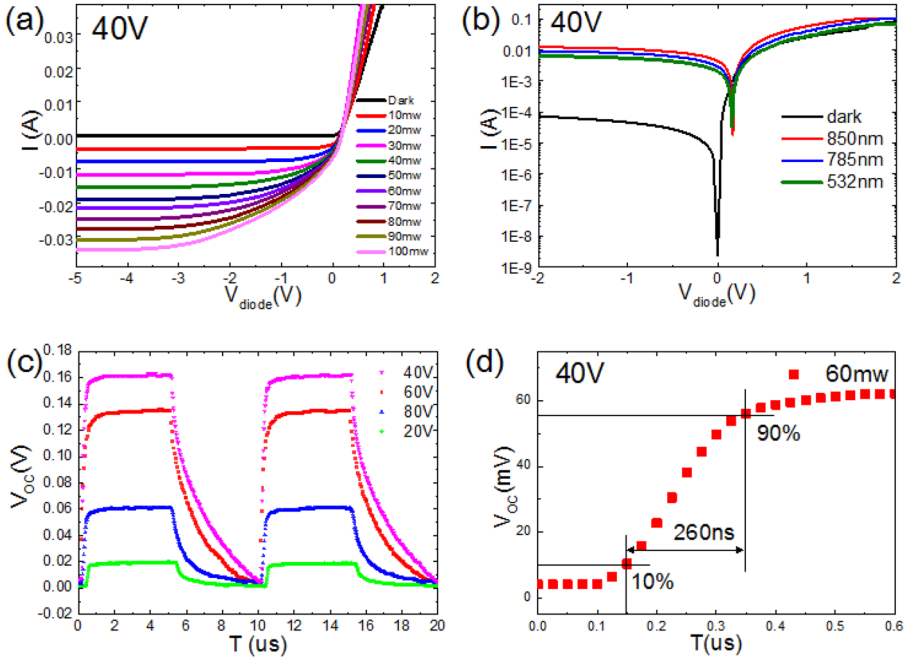

Figure 2. a) *I–V* curves of 40 V GNEC film in darkness and under illumination of 785 nm laser for various incidental powers. b) *I–V* curve of a 40 V GNEC film in the dark and under 532, 785, 850 nm laser illumination for 40 mW incidental powers. c) Frequency response of a 100 KHz optical signal of 40 mW at a V_{dep} of 20, 40, 60, and 80 V under 785 nm laser illumination. d) Time response of a 100 KHz optical signal of 60 mW under 785 nm laser illumination.

Table 1. Comparison of response time (rise time) of our device and other reports. The rise time (t_r) was defined as the time taken by the photocurrent to go from 10 to 90% of its final steady state value.

Several typical graphene/silicon photodetectors	Response time (t_r)
Graphene-silicon[28]	A few milliseconds
Graphene double-layer heterostructure[30]	1 ms
Perovskite-graphene[31]	87 ms
Graphene/n-Si[32]	0.32 ms
GNEC/p-Si (this work)	260 ns

states, and thus generate a stronger photocurrent under illumination.

As shown in Figure 2b, the photocurrent of the GNEC film/p-Si was tested in the dark and under 532, 785, and 850 nm laser illumination for 40 mW incidental powers. GNEC film/p-Si exhibits better photoelectric performance under 850 nm lasers, indicating that it is more sensitive to near-infrared light. The spectral sensitivity of the device will be investigated later. At zero bias, the dark current of the heterojunction can be as low as 2×10^{-9} A, showing a small leakage, which is attributed to the increase in the barrier due to the downward shift of the Dirac point. In addition, under the 850 nm laser irradiation, the ON/OFF radio can reach to 10^7. The correlation between specific detectivity (D^*) and the noise equivalent power (NEP) can be expressed as: $D^* = A^{1/2}/\mathrm{NEP}$, where A is the area of the photodetector (0.25 cm^2), Δf is the electrical bandwidth (commonly 1 Hz). The D^* of 40 V GNEC film reaches to 1.34×10^{12} Jones and the NEP is as small as 186 $pW/Hz^{1/2}$ under 850 nm laser without external bias. The bias-free D^* of our device is higher than 7.69×10^9 Jones of biased Graphene/n-Si photodetector.[27] This is due to high responsivity and the low dark current at $V_{diode} = 0$ V enabled by the natural pn junction of self-n-doped GNEC film and p-Si.

As shown in Figure 2c, the optical response speed of the GNEC film/p-Si was tested at a frequency under 100 kHz. The response time of the GNEC film/p-Si is only 260 ns (Figure 2d). In previous studies, photodetectors of high photoresponsivity are often accompanied by a delay in photo response time (**Table 1**).[28–31] Unlike other materials, GNs in GNEC films play an important role in charge transport. Since the high-density GN is vertically grown on the GNEC film, the charge transport path is maintained.

As shown in **Figure 3**a–d, we prepared GNEC film at $V_{dep} = 20$, 40, 60, and 80 V, and tested their photocurrent responsivity from 300 to 1100 nm. GNEC film/p-Si exhibits better photocurrent responsivity under reverse diode bias ($V_{diode} = -2$ V). The GNEC films show a broadband responsivity from blue to NIR region. As the V_{dep} increases, the crystallinity of the carbon film increases, and the average GN width increases. The R peak appears at 841 nm light of 40 V film, while R peaks are around 910 nm of 60 and 80 V films. This is because the larger-width GN has smaller band gap energy. The photocurrent responsivity of GNEC film/p-Si increased from 0.126 A W^{-1} at 20 V to 0.401 A W^{-1} at 40 V, and then decreased to 0.279 A W^{-1} at 60 V, further reduced to 0.194 A W^{-1} at 80 V. The responsivity is strongly dependent on the density of edge (N_{edge}). At 20 V, the film structure is amorphous. The a-C film has no N_{edge}. The photoelectric performance is the lowest. As V_{dep} increases to 40 V, small-size (≈3 nm in TEM) GNs were formed among the carbon film. In a certain film area, the amount of small-size GNs is more than that of large-size GNs. Thus, N_{edge} of small-size GNEC film is considerably high. As the V_{dep} increases to 60 and 80 V, the crystallinity and GN size increases

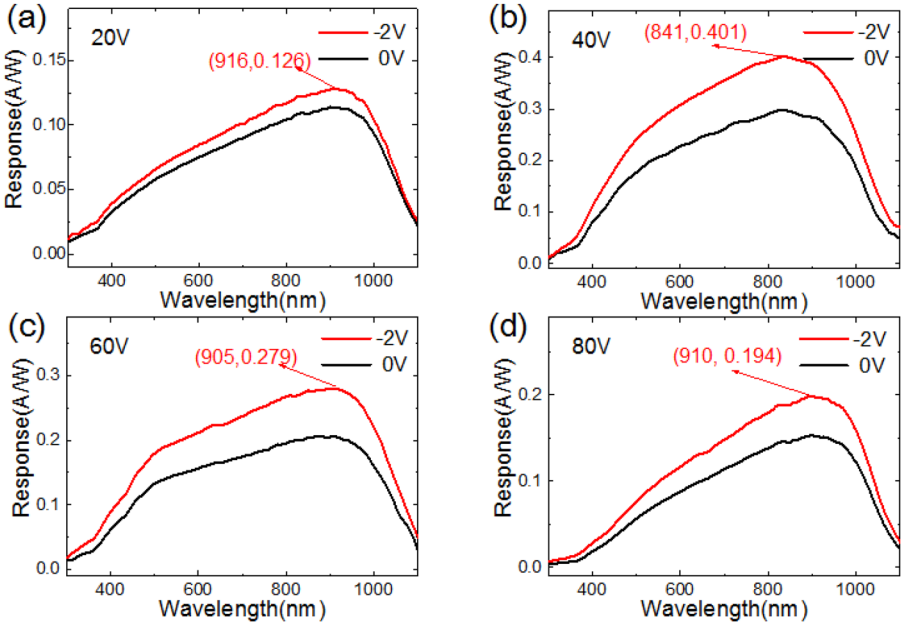

Figure 3. Spectral response curves (from 300 to 1100 nm) of films at V_{dep} of (a) 20 V, (b) 40 V, (c) 60 V and (d) 80 V. The spectral response curves were measured under $V_{diode} = 0$ and −2 V. The peak value (R) and position (wavelength) of each film was marked.

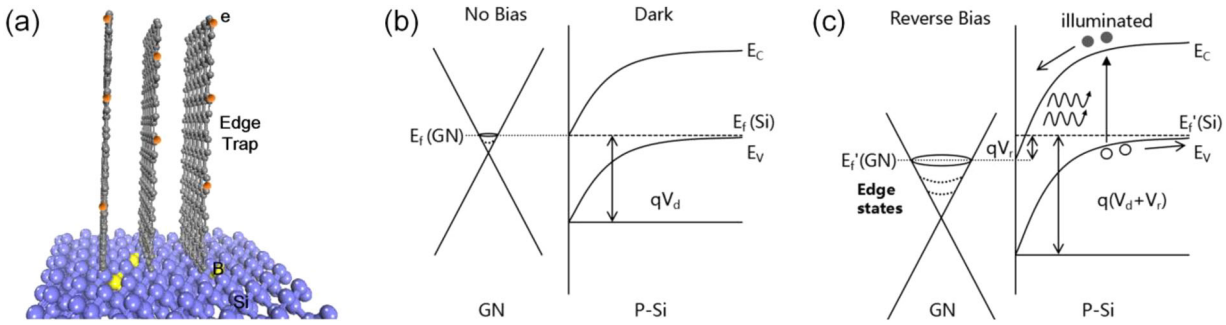

Figure 4. a) The process of edge capturing photoelectrons. b) Energy band structure diagram of GNEC film/p-Si heterojunction at zero bias in dark state. c) Energy band structure diagram of GNEC film/p-Si heterojunction under reverse bias in illumination.

(≈12 nm). The N_{edge} of large-size GNEC films decreases, resulting in a decrease in the photocurrent responsivity. The positive correlation between R and N_{edge} is determined by the edge quantum trapping of photo-excited electrons which will be discussed later.

Figure 4a illustrates the edge quantum trapping of photo-excited electrons. The edges of standing structured GN serve as electron trapping centers due to the edge bond contraction and potential well depression. As shown in Figure 4b, edge states of GN locate at the E_f traps excess electrons and raise the E_f(GN). The E_f(Si) of p-Si locates near the valence band (E_v) and bends at the interface with a Schottky barrier qV_d. Figure 4c shows the Fermi level of GN (E_f(GN)) and p-Si (E_f(Si)) when a reverse bias voltage V is applied to p-type silicon. The reverse bias causes the GN Dirac to move down, resulting in N-type behavior of the GN. In the case of non-equilibrium, the quasi-Fermi level is formed separately for the holes of p-Si (E_f'(Si)) and the electrons of GN (E_f'(GN)). An applied reverse-bias can lift up the E_f'(GN) with respect to Dirac point, opening up a large number of accessible states for electrons to inject from Si. In addition, the drop of the Dirac point increases the barrier by qV_r, which effectively reduces the dark current. Under illumination, when photoexcited carriers appear at the interface between the GNEC film and the p-Si substrate, the edges of the graphene nanosheets act as the capture center for the photoexcited electrons. Once the photoexcited charge is separated by the built-in potential (V_{bi}) of the GNEC film/p-Si, the high-density GN edge of the GNEC film will rapidly capture the photoelectrons, thereby reducing the recombination of photoelectrons with holes on GNEC film and effectively increasing charge carrier lifetime.

Apart from the bias V_{dep}, other factors would also affect the performance of the GNEC films. For example, as the electron flux of Ar plasma increases from $0.49\Phi_0$ to $1\Phi_0$ ($\Phi_0 = 2.57 \times 10^{21}\,mm^{-2}\,s^{-1}$), I_D/I_G increases 1.11–1.28 of 80 V GNEC film, indicating the crystallization enhanced by electron flux.[33] The irradiation time also affects the thickness of the GNEC film. Nitrogen-doped graphene is also a quite interesting issue. Nitrogen can donate electrons to graphene and provide extra quantum states at the Fermi level.[34] It can be expected that the N-doping should enhance the performance of GNEC film.

In summary, graphene nanocrystallites grown vertically on GNEC films can significantly improve photoelectric performance by increasing the ability to collect photogenerated electrons and prolonging the lifetime of photoexcited carriers. Compared to conventional a-C films, GNEC films coated on p-Si exhibit excellent photocurrent responsivity ($0.401\,A\,W^{-1}$) and high sensitivity response time ($\tau_{rise} = 260$ ns) under reverse bias. High specific detectivity (1.34×10^{12} Jones) was obtained at zero bias. By adjusting V_{dep}, the nanostructure of GNs on GNEC can be controlled to form a higher N_{edge} to improve photoelectric performance. The outstanding performance of the GNEC film and the clarification of the GN edges functioning as trapping centers in the photovoltaic process will benefit not only the practical applications of the novel device but also the fundamental understanding of edge quantum trapping. GNEC film/p-Si heterojunction photodetectors can be produced at low cost, large area, and easy to transfer, which has a promising application in industrial production.

Acknowledgments

The Electron Microscope Center (EMC) of Shenzhen University is kindly acknowledged for instrument time and technical support. This work was supported by National Natural Science Foundation (Nos. 51605306, 11605115) of China, Natural Science Foundation of Guangdong (No. 2016A030310060) and of Shenzhen (No.827000131), Shenzhen foundation fund (No. JCYJ20160427105015701).

Conflict of Interest

The authors declare no conflict of interest.

Keywords

carbon films, edge quantum trapping, graphene nanocrystallites, heterojunctions, photoelectric response

Received: September 26, 2018
Revised: December 3, 2018
Published online:

[1] T. Nishimura, H. Sugiura, K. Nakada, A. Yamada, *Phys. Status Solidi RRL – Rapid Res. Lett.* **2018**, *12*, 1800129.

[2] Y. Yue, C. Shao, F. Wang, Y. Wang, W. Chen, L. Hu, *Phys. Status Solidi RRL – Rapid Res. Lett.* **2018**, *12*, 1800100.
[3] S. Srisonphan, W. Kanokbannakorn, N. Teerakawanich, *Phys. Status Solidi RRL – Rapid Res. Lett.* **2015**, *9*, 656.
[4] X. Wan, Y. Xu, H. Guo, K. Shehzad, A. Ali, Y. Liu, J. Yang, D. Dai, C.-T. Lin, L. Liu, H.-C. Cheng, F. Wang, X. Wang, H. Lu, W. Hu, X. Pi, Y. Dan, J. Luo, T. Hasan, X. Duan, X. Li, J. Xu, D. Yang, T. Ren, B. Yu, *npj 2D Mater. Appl.* **2017**, *1*, 4.
[5] D. R. Mckenzie, D. Muller, B. A. Pailthorpe, *Phys. Rev. Lett.* **1991**, *67*, 773.
[6] H. A. Yu, T. Kaneko, S. Otani, Y. Sasaki, S. Yoshimura, *Carbon* **1998**, *36*, 137.
[7] H. A. Yu, Y. Kaneko, S. Yoshimura, S. Otani, *Appl. Phys. Lett.* **1996**, *68*, 547.
[8] K. M. Krishna, M. Umeno, Y. Nukaya, T. Soga, T. Jimbo, *Appl. Phys. Lett.* **2000**, *77*, 1472.
[9] H. A. Yu, Y. Kaneko, S. Yoshimura, S. Otani, *Appl. Phys. Lett.* **1998**, *68*, 547.
[10] V. S. Veerasamy, G. A. J. Amaratunga, J. S. Park, W. I. Milne, H. S. Mackenzie, D. R. Mckenzie, *Appl. Phys. Lett.* **1994**, *64*, 2297.
[11] Q. Xue, S. Wang, J. Li, H. Zhang, Z. Jiao, *Phys. Status Solidi A* **2012**, *209*, 1359.
[12] M. Ma, Q. Xue, H. Chen, X. Zhou, *Appl. Phys. Lett.* **2010**, *97*, 061902.
[13] Q. Xue, M. Ma, Y. Zhen, X. Zhou, S. Wang, *Diamond Relat. Mater.* **2012**, *21*, 24.
[14] X. Zhang, Y. Nie, W. Zheng, J.-l. Kuo, C. Q. Sun, *Carbon* **2011**, *49*, 3615.
[15] X. Liu, X. Zhang, M. Bo, L. Li, H. Tian, Y. Nie, Y. Sun, S. Xu, Y. Wang, W. Zheng, C. Q. Sun, *Chem. Rev.* **2015**, *115*, 6746.
[16] Y. Zhang, T. Liu, B. Meng, X. Li, G. Liang, X. Hu, Q. J. Wang, *Nat. Commun.* **2013**, *4*, 1811.
[17] W. Zhang, D. Diao, K. Sun, X. Fan, P. Wang, *Nano Energy* **2018**, *48*, 456.
[18] C. Wang, X. Zhang, D. Diao, *Nanoscale* **2015**, *7*, 4475.
[19] C. Wang, D. Diao, *Carbon* **2016**, *112*, 162.
[20] P. Wang, W. Zhang, D. Diao, *Surf. Coat. Technol.* **2017**, *332*, 153.
[21] X. Zhang, C. Wang, C. Q. Sun, D. F. Diao, *Appl. Phys. Lett.* **2014**, *105*, 042402.
[22] W. Chen, X. Zhang, D. Diao, *Appl. Phys. Lett.* **2017**, *111*, 114105.
[23] Z. L. Wang, *J. Phys.: Condens. Matter* **2004**, *16*, 829.
[24] A. C. Ferrari, J. C. Meyer, V. Scardaci, C. Casiraghi, M. Lazzeri, F. Mauri, S. Piscanec, D. Jiang, K. S. Novoselov, S. Roth, *Phys. Rev. Lett.* **2006**, *97*, 187401.
[25] M. A. Pimenta, G. Dresselhaus, M. S. Dresselhaus, L. G. Cançado, A. Jorio, R. Saito, *Phys. Chem. Chem. Phys.* **2007**, *9*, 1276.
[26] P. Venezuela, M. Lazzeri, F. Mauri, *Phys. Rev. B* **2011**, *84*, 035433.
[27] L. Fangze, K. Swastik, *ACS Nano* **2014**, *8*, 10270.
[28] X. An, F. Liu, Y. J. Jung, S. Kar, *Nano Lett.* **2013**, *13*, 909.
[29] L. Yang, G. Hu, D. Zhang, D. Diao, *Appl. Phys. Lett.* **2016**, *109*, 1461.
[30] C. H. Liu, Y. C. Chang, T. B. Norris, Z. H. Zhong, *Nature Nanotechnol.* **2014**, *9*, 273.
[31] Y. Lee, J. Kwon, E. Hwang, C.-H. Ra, W. J. Yoo, J.-H. Ahn, J. H. Park, J. H. Cho, *Adv. Mater.* **2015**, *27*, 41.
[32] X. M. Li, M. Zhu, M. D. Du, Z. Lv, L. Zhang, Y. C. Li, Y. Yang, T. T. Yang, X. Li, K. L. Wang, H. W. Zhu, Y. Fang, *Small* **2016**, *12*, 595.
[33] A. C. Ferrari, J. Robertson, *Phys. Rev. B* **2000**, *61*, 14095.
[34] J. Li, L. Lin, D. Rui, Q. Li, J. Zhang, N. Kang, Y. Zhang, H. Peng, Z. Liu, H. Q. Xu, *ACS Nano* **2017**, *11*, 4641.